JOURNAL OF MATERIALS SCIENCE 16 (1981) 2369–2380

Correlation of electrostatic charging patterns with internal structure in diamonds

R. C. G. ADAM, T. A. BIELICKI, A. R. LANG
H. H. Wills Physics Laboratory, University of Bristol, Bristol, UK

The methods described by DeVries and Tuft [1] for revealing inhomogeneities in diamonds by applying xerographic techniques to their polished surfaces have been developed and tested on a small suite of diamonds known to cover a wide range of impurity-dependent properties. These specimens had all been characterised by one or more of the following methods: infra-red absorption, bi-refringence, ultra-violet absorption topography, X-ray topography and cathodoluminescence topography. In general the charge pattern, as revealed by retention of a superficial deposit of a fine powder, could be correlated well with known inhomogeneities outcropping at the specimen surface. In one case, however, the dust pattern disclosed unsuspected zones of low-level radiation damage in a specimen that had been irradiated by a supposedly well-collimated proton beam.

1. Introduction

Recently DeVries and Tuft [1] have presented an intriguing account of a useful technique for revealing inhomogeneities in diamond crystals when such inhomogeneities are intersected by a polished surface of the specimen. They electrostatically charged the specimen surface and detected non-uniformitites in the surface charge distribution adopted by the retained charge. This pattern could be rendered visible by dusting the charged surface with a finely-divided powder which adhered to the surface in a non-uniform fashion as a consequence of the non-uniform electrostatic field conditions prevailing thereon. Most of the patterns on synthetic crystals exhibited by DeVries and Tuft show a geometry explicable simply by the distribution of growth sectors of the major forms {1 0 0} and {1 1 1}, with possible presence also, in weak development, of the minor forms {1 1 0} and {1 1 3}. (The latter forms, even when very weakly developed, are readily picked out in cathodoluminescence topographs [2].) The single natural diamond pictured by DeVries and Tuft presented a complex pattern, reminiscent of some that have been encountered in etching experiments (e.g. Fig. 4 of [3]).

The correlation of dust patterns with known types of internal inhomogeneity in diamonds was the primary aim of this study. A further aim was to explore means for improving the sensitivity, contrast and reproducibility of the technique, with the hope of gaining understanding of the dominating processes and specimen parameters involved. A certain impetus was gained from the statement by DeVries and Tuft that of the approximately 50 natural cut stones they had examined, only a few had shown a useful pattern on the as-polished facets. The object of this work was to produce dust patterns on natural specimens of no less contrast than those achieved on synthetic specimens by DeVries and Tuft.

The use of powder deposition patterns for delineating domain patterns on the surfaces of ferromagnetic and ferroelectric materials is well-established. The powders are usually dispersed in a liquid, as in the Bitter technique for ferromagnets (see for example [4]), and also as in the case of dielectric powders dispersed in insulating organic liquids used for studying ferroelectric domains (e.g. sulphur or Pb_3O_4 in hexane [5]). Indeed, for certain ferroelectrics, a high-resolution dew-drop deposition technique that involves no solid medium has been described [6]. Experiments on diamonds have to be made without assistance

0022–2461/81/092369–12$03.20/0

from permanent polarization (excluding a hypothetical possible contribution from microscopic inclusions), and with the small and transient forces available it is likely that the agitation accompanying evaporation of a liquid vehicle would militate against sensitivity and reproducibility of the powder deposition pattern; however, this question deserves investigation. Apart from an exploratory experiment with liquid crystalline material, all the work described below was conducted with both the powder and the specimen surface dry: the techniques were truly xerographic.

2. Experimental procedure

2.1. Charging techniques

Very many variations of technique were tried, and it was found that the method which best suited one type of diamond, or which revealed one type of feature, was not necessarily the best technique for observing another specimen or feature. The simplest of all the methods uses triboelectricity. In order to perform triboelectric charging in a controlled fashion, the rubbing was done by a pad of tissue attached to the spindle of a small motor-driven buffing machine. Although the simplest, this was the least satisfactory of all the charging techniques, and only one example of its application is here shown (Fig. 3d), in order that it may be compared with the other techniques.

It was anticipated that control of the ambient humidity would be necessary. For this purpose the specimen and electrodes were enclosed in a plywood box, measuring about 12 cm by 15 cm by 30 cm, set up with long axis vertical. The box could be flushed with dry nitrogen. The powder was contained in a rubber balloon attached to an inlet tube near the top of the box; after shaking the balloon to disturb the powder, the latter could be introduced into the box by gently puffing from the balloon. In the box, the specimen was mounted at the centre of a polished aluminium disc electrode 8 cm in diameter which was supported in a vertical plane close to one of the larger vertical sides of the box by means of an insulated spindle. Opposite this electrode was a large glass window through which the specimen was illuminated, observed and photographed. A second aluminium disc electrode, attached to a pivot, could be swung in front of the first disc, to form the configuration of a parallel-plate condenser with a spacing of about 1 cm. After application of a potential of up to 6 kV between the electrodes, the movable electrode was swung away again, leaving an induced charge on the specimen and allowing observation to be resumed. In an alternative arrangement only the base electrode was used, held at a constant potential, and the powder could be introduced either while the potential was applied, or after disconnection of the voltage supply. In other charging procedures, corona-charging devices were used. One such device consisted of a single pointed wire, held at -10 kV relative to earth potential, surrounded by an insulating ring which was itself surrounded by an earthed cylindrical conductor. Other devices consisted of multiple pointed wires at high potential. These corona devices could also be swung in front of the specimen in the box, the specimen being earthed or held at a potential of $+5$ kV. When experiments were performed in the open, the corona device was simply waved over the diamond; following this, the diamond, fixed rigidly to its mount, held by Sellotape, or held by tweezers, was dusted, for example by dipping it into the dust-cloud within a jar that had been shaken. Specimen mountings of numerous types were used, ranging from well-conducting, as when the diamond was mounted with colloidal graphite directly on to the electrode, to insulating, as when the diamond was mounted with Sellotape to a wooden backing. A black backing facilitated photography of the dust patterns. A variant sometimes beneficial involved surrounding the diamond with a silicone rubber compound which extended so as to be flush with its front surface.

2.2. Choice of powder

The following materials in powder form were tried: Xerox toner, French chalk, flour, cinnamon, ground rice, sulphur, animal charcoal, Cr_2O_3, $BaTiO_3$, TiO_2, ZnS, Fe_3O_4, Al_2O_3, Pb_3O_4, MgO and a magnetic tape developer ("Vulture Video Verifier"). Employment of the first and last listed was prompted by the experience of DeVries and Tuft; but whereas the tape developer (a finely-divided iron/iron-carbide preparation) proved to be one of the best powders, the Xerox toner stuck indiscriminately to everything and was not useful. When deemed necessary, the powders were ground, dried and passed through a 400 mesh sieve (opening diameter 38 μm). The principal causes of unsatisfactory powder behaviour appeared to be either insufficiently small particle size (as in the case of the sulphur and ZnS powders used) or

subsequent particle clumping. The $BaTiO_3$ and TiO_2 powders grew long filaments. The animal charcoal produced poor contrast because of its blackness. The grey Fe_3O_4 precipitate powder was also inferior because of low contrast. Ultimately, efforts were concentrated on experiments with the tape developer, with Pb_3O_4 and with MgO. Dusting with MgO was achieved by burning a strip of magnesium ribbon under an inverted funnel and holding the diamond in the smoke column rising from the funnel-spout "chimney".

3. Selection of specimens

A small suite of specimens was chosen whose properties encompassed a considerable range of the highly diverse behaviour of diamonds. The standard classification of diamonds is based upon the nature and strength of impurity-dependent optical absorptions. The principal extrinsic absorption bands are due to nitrogen impurity. This element is also the major known impurity in diamond. An outline of the diamond classification scheme is as follows. (For more detail see an excellent contemporary review of optical absorption and luminescence of diamond by Walker [7].) The great majority of natural diamonds belong to Type Ia which contains nitrogen in amounts up to a few parts per thousand which is present in at least three forms: the so-called "A" and "B" centres, and the platelet precipitates on {1 0 0}. Presence of each form is diagnosed by characteristic infra-red absorption spectra. The platelets are easily seen by transmission electron microscopy, but the "A" and "B" defects have not to date been resolved. Nitrogen is present in a singly-substitutional atomic state in Type Ib: to this class belong common synthetic specimens, but it is very rarely represented in natural specimens. When the nitrogen content drops below ~ 10 ppm, the ultra-violet absorption between ~ 330 nm and ~ 220 nm (which in Type Ia is attributed largely to "A" centres) becomes insignificant. The purest naturally occurring diamonds are the semiconducting Type IIb diamonds. These contain typically 0.5 ppm boron, with electrically active nitrogen below the 0.1 ppm level. The electrical resistivity of Type IIb diamonds usually ranges from 10^3 to 10^5 ohm m, but that of Types IIa, Ia and Ib is many orders of magnitude higher, ranging up to values in excess of 10^{18} ohm m in the case of the latter two types. These resistivity figures relate to measurements taken in the dark; Type Ib synthetic specimens are reported to exhibit photoconductivity with a low-energy threshold around 2 eV (620 nm), and Type Ia containing nitrogen in "A" form to do so at a threshold of 4 eV (310 nm) [8].

It is quite common to find Type Ia specimens with narrow growth zones of Type IIa material intercalated within them. The first crystal to be described in Section 4 below, Specimen GH2, is a much-studied representative of this class. It has been examined by ultra-violet topography, Bragg reflexion and diffuse reflexion X-ray topography [9], and by cathodluminescence topography [10].

In synthetic specimens faceted growth on both {1 1 1} and {1 0 0} is usual, often with {1 0 0} dominant, but in natural crystals true {1 0 0} facets are very rare. However, perhaps up to 1% of natural crystals exhibit transient, minor developments of a non-faceted mode of growth which takes the form of hummocky surfaces of mean orientation {1 0 0}: this non-faceted growth was first disclosed by etch patterns [3, 11, 12], and has been studied by X-ray topography, light-scattering, bi-refringence, and cathodoluminescence topography [13–15]. Sometimes non-faceted, "cuboid" growth becomes as well-developed as, or even dominant over faceted {1 1 1} growth. A good example of naturally occurring mixed-habit growth, Specimen GDO2, was included in the present study.

To represent synthetic diamonds, a large experimental crystal, Specimen L_2, was chosen. This had earlier been studied by X-ray topography and cathodoluminescence topography in the visible spectrum [2], and more recently the polarization of the near infra-red cathodoluminescent emission from its {1 1 1} growth sectors has been reported [16].

A natural semiconducting, Type IIb specimen completed the suite. This specimen had been proton-irradiated by a pinhole-collimated beam to produce small patches of radiation damage. Before its dust patterns were observed, only its bi-refringence pattern had been recorded. The unexpected findings from the dust patterns were subsequently confirmed by cathodoluminescence topography. (It was not a good subject for X-ray topography since it was a mosaic crystal, with high dislocation density.) All the specimens discussed in this work had at least one pair of large, opposite, polished faces which facilitated photographic recording of the dust patterns.

4. Observations

4.1. Natural Type Ia diamond containing Type IIa growth zones

This specimen, Specimen GH2, has faces of size 6 mm by 5.3 mm and is 0.42 mm in thickness. Fig. 1a to d shows patterns on the face designated "a". Fig. 2 shows a simplified map of features observed in Fig. 1a to d. Fig. 3a to d shows the opposite face, "b", with Fig. 4 as key. Figs 3 and 4 are printed left-to-right to facilitate comparison of growth-zone outcrops on the two faces. The upper right-hand side of face "b" is bevelled by a fracture: some reflexion of light from this is seen in Fig. 1a and d, and Fig. 3b and c, and this should be disregarded. Fig. 1a and 3a are monochrome versions of the cathodoluminescence patterns reproduced in colour in [10], where the corresponding surface reflexion X-ray topographs are also shown and details are given concerning the nature and crystallographic orientations of the major features observed. Referring to the maps, Figs 2 and 4, a simplified description of the growth zones runs as follows. The brightly luminescent, inner zone A is rich in platelets and "B"-nitrogen centres. This region is almost completely surrounded by a shell, B, of ultra-violet-transparent, Type IIa material. The matrix of shell B gives negligible visible cathodoluminescence, but it does contain luminescent dislocations and platelets (not individually resolved on the scale

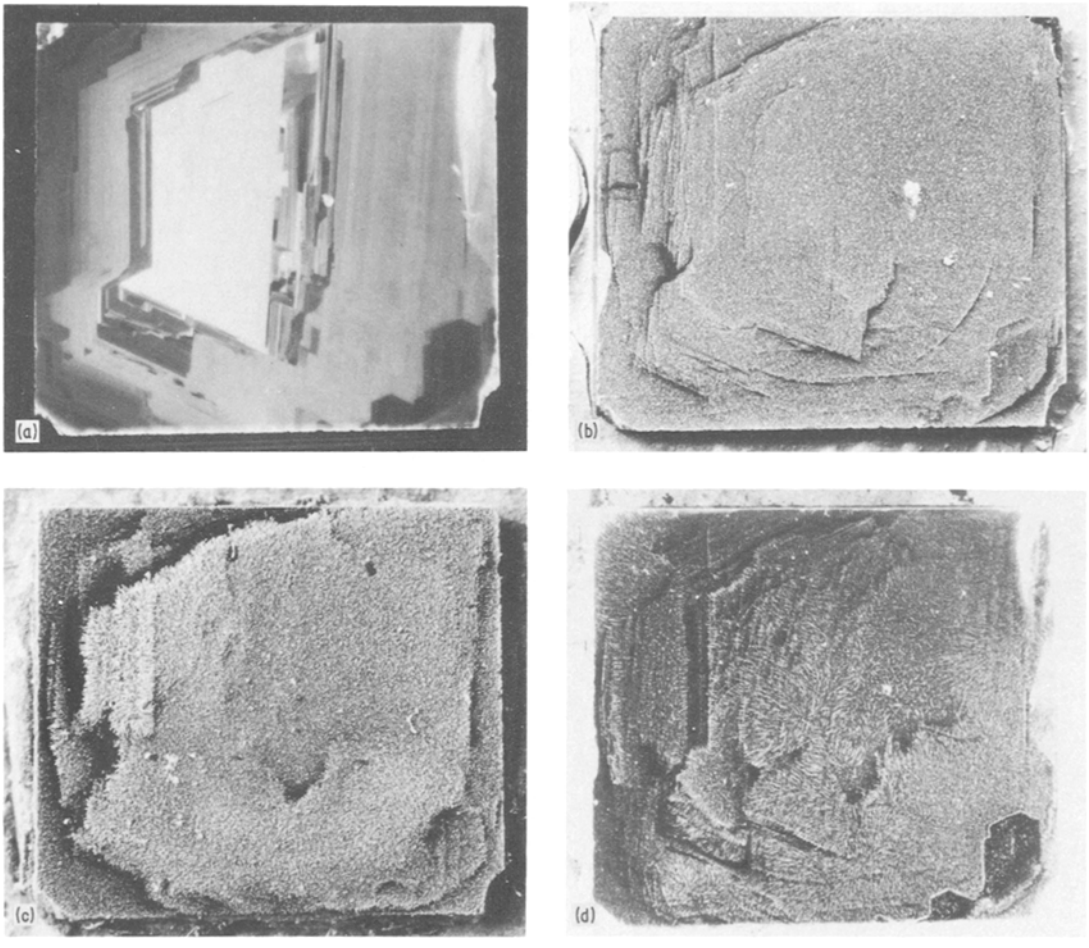

Figure 1 Natural diamond specimen GH2, surface designated "a". Surface orientation close to (1 1 2). The direction [1 $\bar{1}$ 0] is nearly vertical in the figure. (a) Cathodoluminescence topograph; (b) Pattern obtained with magnetic tape developer after corona charging of the specimen by a pointed electrode at − 10 kV while the specimen was held in tweezers; (c) Pb_3O_4 pattern: Specimen mounted on colloidal graphite backing separated from the metal electrode base by a 1 mm layer of "Blu-Tack", powder desposited while the electrode was held at + 5 kV; (d) MgO pattern: specimen mounted on Sellotape and corona charged as in (b) then held in MgO smoke for 3 seconds. Note low level of dust accumulation in zone D, and enhanced accumulation on C–D boundary.

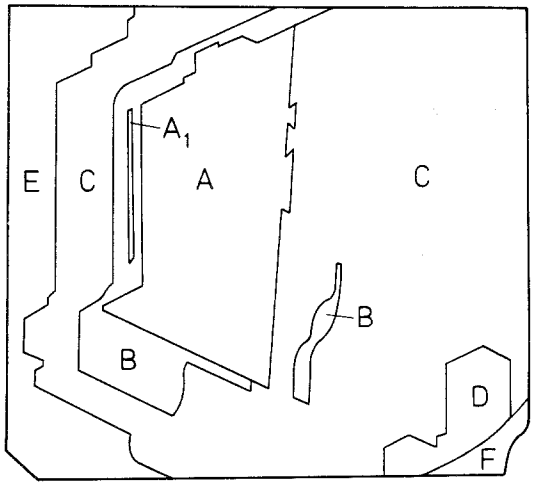

Figure 2 Key to the major features in Fig. 1, explained in text.

of these figures). Also, within B are intercalated some thin layers of material akin to that in zone A. Certain of these layers are numbered in Figs 2 and 4 (A_1–A_4). Surrounding B is a zone of a more ultra-violet-opaque material, C, which, in the left-hand margins, is followed by an even more ultra-violet-opaque zone, E. In the lower right-hand corner is another "window" of ultra-violet-transparent, Type IIa material, D, which is bounded on the outside by a curved surface separating it from the zone F. It is not known whether this curved surface arises from post-growth solution or is a local manifestation of non-faceted growth. The corner zone, F, is strongly ultra-violet-absorbing, and may correspond to the zone E intersected on the left-hand side of the specimen. Between C and E there are

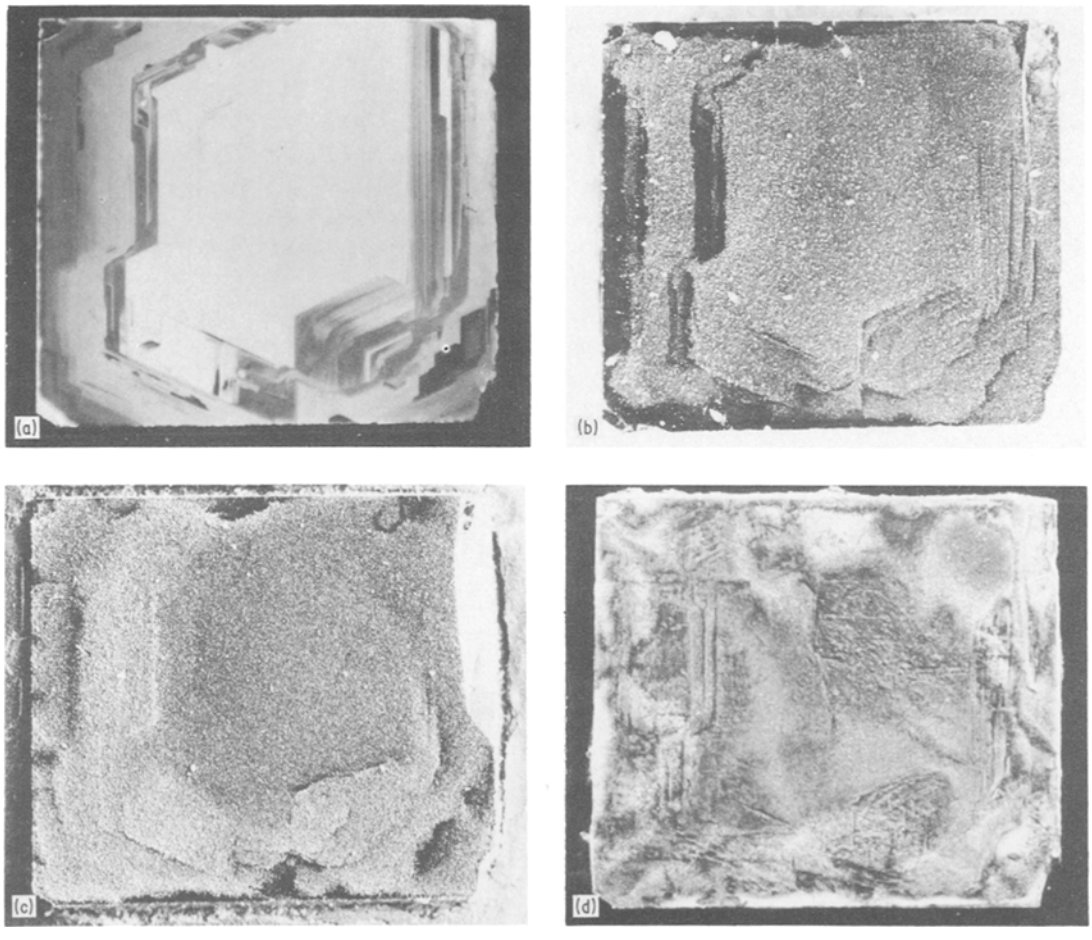

Figure 3 Natural diamond specimen GH2, surface designated "b". Photographs printed left-to-right to assist comparison with Fig. 1. (a) Cathodoluminescence topograph; (b) Magnetic tape developer pattern after corona charging as in Fig. 1b, specimen mounted on silicone rubber compound; (c) Pb_3O_4 pattern obtained in a similar way to that shown in Fig. 1c; (d) MgO pattern obtained after triboelectric charging of specimen.

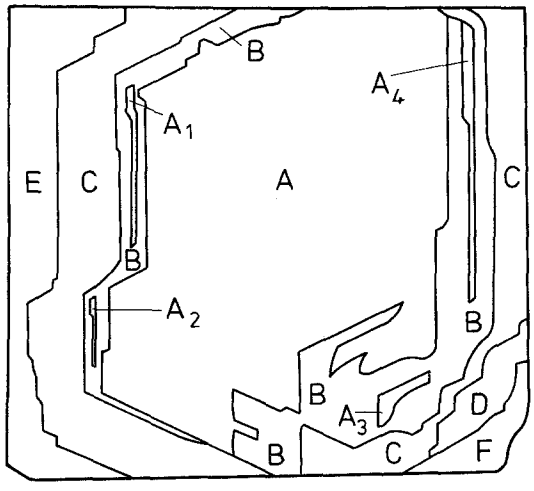

Figure 4 Key to the major features in Fig. 3.

a few very small ultra-violet-transmitting, Type II "windows". These are not indicated on the maps, Figs 2 and 4, but can be seen in Fig. 9 of [9].

None of the dust patterns shows detail that approaches the richness of detail found in the cathodoluminescence patterns, Figs 1a and 3a, but some of the dust patterns do pick out, at least locally, certain fine structures with remarkable sensitivity. Unless otherwise stated, the patterns here exhibited are typical examples pertaining to the powder and charging technique employed. (The charging technique is specified in the figure captions.) Some principal correlations are as follows. The Type II zones B and D stand out well in dustings performed without a high voltage applied to the base of the crystal, i.e. under conditions when rate of charge leakage from the dusted surface is expected to be the dominating contrast-producing factor. This is not unexpected, for the Type II zones are believed to have a lower resistivity than the impurity-rich zones surrounding them, and both B and D run through the specimen from surface "a" to surface "b". It is known from X-ray topography that zone B is dislocation-rich whereas zone D has few dislocations, but no obvious difference in dust pattern behaviour results therefrom. The amount of detail revealed varied from dusting to dusting. For example, Fig. 3b, in which dusting was relatively light on the left-hand side, gives high overall contrast of zone B on the left. With more powder, details within B, i.e. the layers A_1 and A_2, could be well resolved. Which particular zone boundaries showed up best depended upon the amount of powder used, as well as upon its nature and the charging technique. As earlier mentioned, triboelectric charging was not a preferred technique, but the example shown, in Fig. 3d, in which the powder deposit is rather thick, does show fine structure with high contrast in some areas, especially in zone B on both the left- and right-hand sides of the photograph. The dusting with Pb_3O_4, performed with high voltage applied to the base of the specimen, appears to be best in discriminating between zones C and E. There are also indications that it can pick out the small Type II "windows" between C and E. (These could be detected with the tape developer.) Perhaps the most unexpected revelation of detail is in zone D on surface "a". Running vertically down the centre of this zone are two narrow bands giving a very faint, yellowish cathodoluminescence which is believed to come from {0 0 1} platelets (not individually resolved). These bands are quite clearly shown in Fig. 1c, and they could also be detected with other powders.

4.2. Natural Type Ia diamond exhibiting mixed-habit growth

Some very strange crystal growth phenomena are encounted in natural diamonds which have crystallized in a combination of the normal {1 1 1} form together with the non-faceted "form" of rounded growth surfaces of near-{1 0 0} orientation which are termed "cuboid". Examples showing the variety and complexity of relative development of these forms have been presented in a review of such mixed-habit growth behaviour [14]. A well-polished slice cut from one of the crystals (GDO2) described in [14] was used in the present experiments. This crystal was chosen because its {1 1 1} and cuboid growth sectors were unusually uniform in defect content, being untypically free from the fine-scale zoning of impurity content that is an even more prevalent characteristic of mixed-habit natural diamonds than of normal octahedrally grown crystals. Crystal GDO2 provided excellent specimen material with which to test whether dust patterns could distinguish between {1 1 1} and cuboid growth. Indeed, the slice of GDO2 used was especially appropriate for such purposes since it contained small columns of {1 1 1}-faceted growth inserted within cuboid matrices. These columns had developed on {1 1 1}-faceted re-entrants located at notches on the boundaries between adjacent, large sectors of non-faceted growth [15].

X-ray topographs (Figs 5a and 6a) can differen-

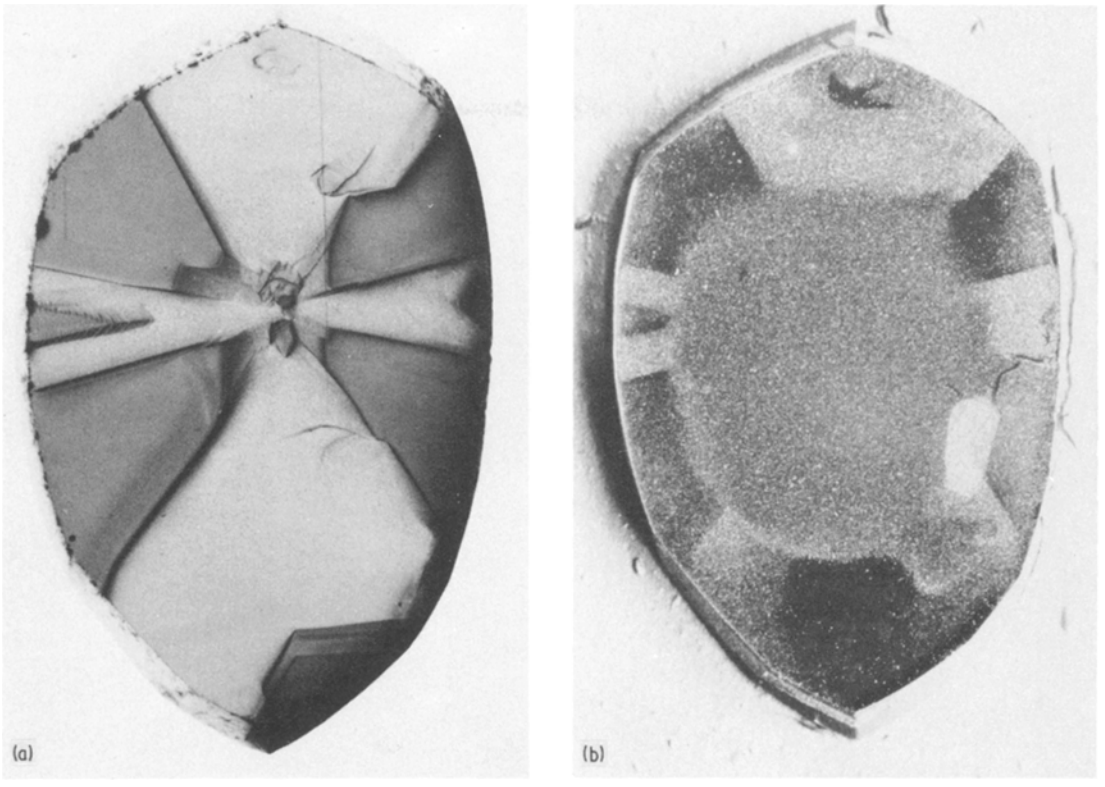

Figure 5 Natural diamond exhibiting mixed-habit growth. Central slice cut from specimen, slice surfaces polished parallel to (1 1 0). Slice of height 6.8 mm and thickness 0.59 mm. (a) Surface reflexion X-ray topograph (Cu$K\alpha$, radiation, reflexion $\bar{1}\,3\,\bar{1}$). (b) Magnetic tape developer pattern obtained 1 second after corona charging with pointed electrode held at — 10 kV, specimen mounted on Sellotape on earthed metal base. (The light patch on the right, below centre, is an artefact arising during drying of the colloidal graphite used for remounting the specimen for photography.)

tiate so clearly between the {1 1 1} and the cuboid growth sectors that labelling of the sectors is superfluous. (However, a key to the face shown in Fig. 5a is given in [15], and diagrams which assist interpretation of the shapes of growth sectors as they outcrop on the surfaces of near-central sections of mixed-habit crystals can be found in [13] and [14].) The {1 1 1} sectors show relatively dark on the prints of the X-ray topographs because of the higher integrated reflexion from the matrix of {1 1 1} growth material compared with that from the matrix of "cuboid" growth material. This increase arises from the presence of a dense, unresolved population of platelet defects in the {1 1 1} sectors. It is currently accepted [7] that the strength of the infra-red absorption at 1365 cm^{-1} (7.3 μm) is a measure of the total platelet area per unit volume (though a relationship of direct proportionality has not yet been proven). In this specimen the absorption coefficient at 7.3 μm is unusually strong in the {1 1 1} sectors, and it is about three times the value found in the outer zones of the cuboid sectors and four times that found in the inner cuboid region. Another striking difference in texture between the {1 1 1} and cuboid growth sectors is the presence in the inner cuboid regions of a population of microscopic, non-diamond bodies. (This is a generally observed characteristic of cuboid growth [13, 14]. The bodies are detectable as light-scatterers, as individual bi-refringence "stars" and on X-ray topographs as dots of enhanced diffraction contrast arising from strain in the surrounding diamond matrix.)

In common with other mixed-habit natural diamonds whose infra-red absorption spectra have been studied, this specimen contains a greater nitrogen impurity concentration in the {1 1 1} growth sectors than in the cuboid growth sectors: from the infra-red absorption measurements on this specimen the concentration of nitrogen in the form of "A"-centres is about 0.1 atomic per cent in

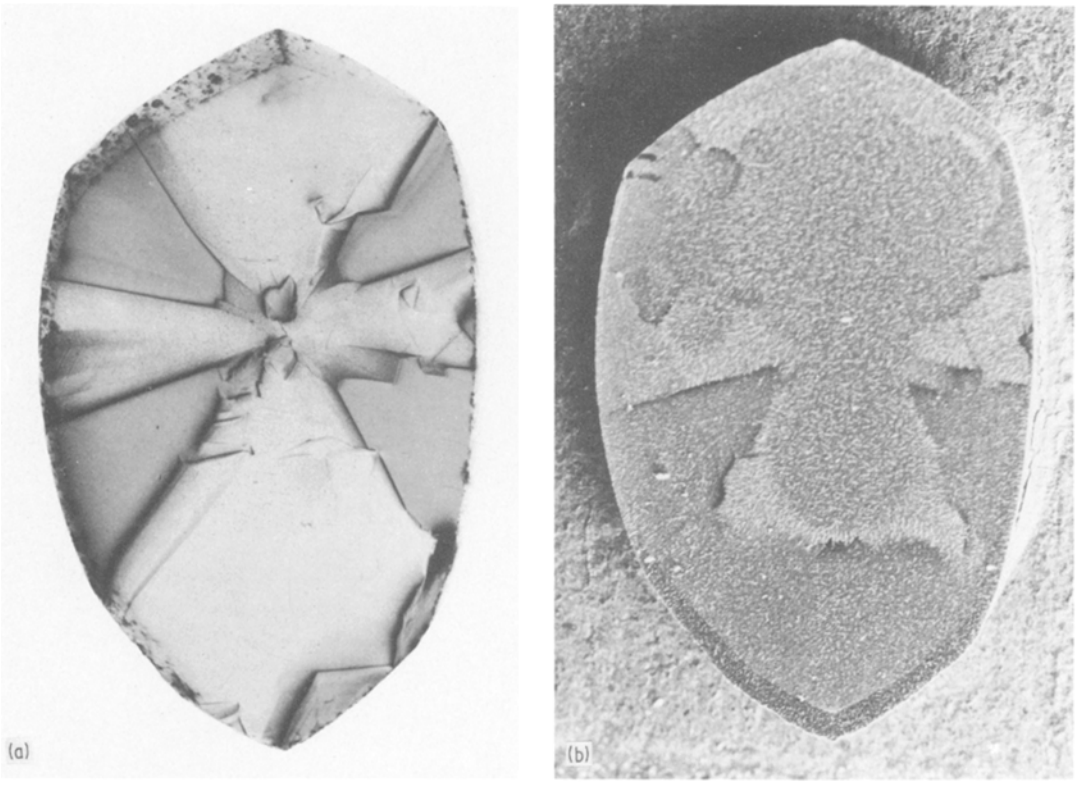

Figure 6 Opposite face of the specimen shown in Fig. 5, photographs printed left-to-right to assist comparison with Fig. 5. (a) Surface reflexion X-ray topograph equivalent to that in Fig. 5a; (b) Magnetic tape developer pattern obtained in a similar way to that shown in Fig. 5b.

the {1 1 1} sectors compared with 0.76 atomic per cent in the cuboid sectors. On the other hand, the cuboid sectors show sharp infra-red absorption peaks at 3107 cm^{-1} and 1405 cm^{-1}. (This is also a usual observation in mixed-habit diamonds [14]). These peaks are attributed to hydrogen impurity, but their relationship with hydrogen concentration is not yet known.

Considering the dust patterns, Figs 5b and 6b, these can be described in simplified terms as exhibiting three levels of powder retention. On the outer parts of the specimen surface there are two levels, low in the {1 1 1} sectors and high in the cuboid sectors, whereas the third, intermediate, level of powder blankets the interior of the surface without revealing the underlying structure. It was only with magnetic tape developer that patterns were obtained which gave a consistently good correlation with the configuration of growth sectors, at least in the outer parts of the specimen, and even with this powder it was found that the interval between charging the surface and dusting it was fairly critical: an interval of about 1 second was found to give the best results. The specimen is, on the whole, believed to be highly insulating. This, together with the relatively large specimen thickness (0.59 mm), would enhance the importance of charge leakage via the surface, relative to charge leakage through the bulk.

The inner zone of intermediate powder density that appears in both Figs 5b and 6b (and which was repeatedly observed) very roughly coincides in limits with the radial limit of the population of visually detectable light-scattering bodies in the cuboid growth zones. It is tempting to grant significance to this observation, but the powder pattern is believed to arise more probably from the restriction to near marginal specimen regions of such combinations of possible leakage paths and electrical field conditions which allowed detection of differences in properties of the diamond matrix. What is clear is that, within this marginal zone, the discrimination between octahedral and cuboid growth is very good. Consider the two "V"-shaped inserts of octahedral growth within the cuboid matrices: the larger "V", which grows out to the

left-hand edge of the specimen at about mid-height, gives a sharp X-ray topograph image in Fig. 5a but only a diffuse image in Fig. 6a. This is because it outcrops only on that face whose X-ray topographic image is shown in Fig. 5a. Appropriately, its dust pattern image appears clearly in Fig. 5b but not at all in Fig. 6b. On the other hand, the much smaller insert of octahedral growth, which expands out to the specimen edge at the same mid-height but to the right-hand side (as seen in Figs 5a and 6a), does outcrop on both faces, and is resolved in both Figs 5b and 6b.

4.3. Synthetic Type Ib diamond

The large specimen L_2 tested was comparable in size with that shown in Fig. 1 of Devries and Tuft [1], but was of irregular shape and presented a much less symmetric and equal development of the {1 0 0} and {1 1 1} forms. In specimen L_2, {1 0 0} was strongly dominant, and sizable intersections with {1 1 1} sectors only occurred close to the peripheries of the two parallel polished faces of the specimen. (The cathodoluminescence topographs and simplified maps of both faces appear in [16].) Many specimen mounting, charging and dusting techniques were tried, all with rather disappointing results. Although it could fairly be claimed that, statistically, differentiation between the {1 0 0} and {1 1 1} sectors was achieved, no individual pattern demonstrated this convincingly. Both surfaces of the specimen contained small outcrops of {1 1 1} facets near their centres. It was hoped to detect these facets, and also the narrow strips of {1 1 0} growth that separated adjacent {1 0 0} sectors, but this was never credibly accomplished. However, there did consistently appear evidence for a central, more conducting region in the specimen, and this coincided roughly with the region containing dense bundles of dislocations (shown in Fig. 7 of [2]). These dislocations are strongly decorated, as is made evident both by light-scattering and X-ray diffraction contrast. The patterns most revealing of matrix inhomogeneities were obtained with corona-charging and MgO smoke, though comparable results were obtained with corona-charging and magnetic tape developer. These patterns showed up the impurity banding parallel to traces of the local growth facet in some {1 0 0} growth sectors, especially in the more peripheral regions of the specimen surfaces. (Banding of this nature is, of course, revealed throughout the {1 0 0} growth sectors by cathodoluminescence topography, and can also be detected by ultra-violet transmission topography in favourably orientated and polished specimen slices [2].)

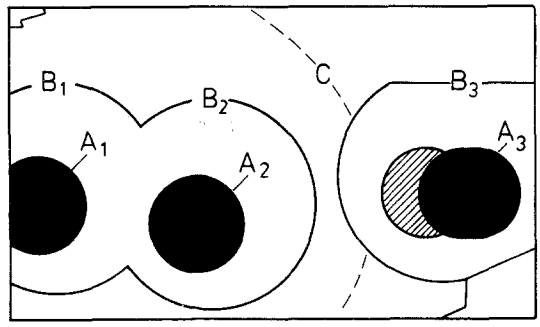

Figure 7 Key to zones of radiation damage on surface of polished block of natural semiconducting diamond (specimen designation SA67F). The patches A_1, A_2 and A_3 are visibly opaque: A_3 overlaps a less-damaged patch, olive-green in colour (shaded). No visible absorption is apparent in the inner penumbral zones bounded by B_1, B_2 and B_3, nor in the outer penumbra bounded by C. The radiation dose within the opaque patches was approximately 1 μA h. The upper left and lower right corners of the surface are truncated by small natural facets whose outlines are sketched, and which can be recognized in Figs 8, 9 and 10.

4.4. Natural semiconducting Type IIb diamond

The representative of this class (kindly lent by Dr Collins, King's College, University of London) was a polished parallelipiped of dimensions 8.8 mm x 5.3 mm x 4.4 mm. Its four large faces each bore a number of small round patches (diameters 0.8 mm to 1.6 mm) of localized radiation damage where it had been bombarded by pinhole-collimated beams of protons of energy 680 kV. These patches ranged from complete opacity for the more heavily irradiated, to olive-green for the more lightly irradiated. The natural colour of the specimen was pale blue in one half (the left half in the key, Fig. 7) and colourless in the other half. Prior to the dusting experiments, the specimen had been examined only by bi-refringence. The bi-refringence pattern indicated a polygonized, mosaic structure (which has also been found in other Type IIb diamonds) upon which a few slip bands parallel to {1 1 1} were superimposed. The large specimen size and high dislocation density suggested that no essential additional information would be gained by X-ray

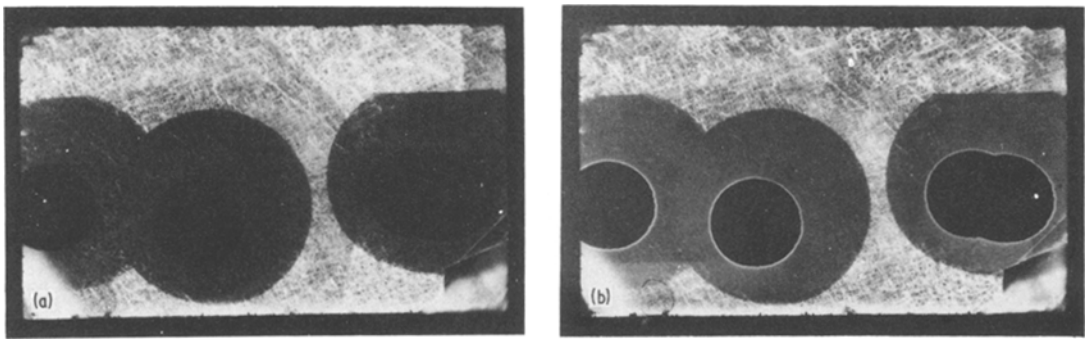

Figure 8 Cathodoluminescence topographs of the surface sketched in Fig. 7. Electron beam energy 30 kV, current density 0.23 μ A mm^{-2}. Photographed on Ilford Pan F film through "anti-haze", ultra-violet-absorbing Kodak-Wratten filter No. 2B. (Flaring in bottom left-hand and right-hand corners arises from reflexions by corner levels on the underside of the specimen.) (a) Additional filtration by Kodak-Wratten filter No. 47B which transmits less than 1% of visible light of wavelengths greater than 490 nm. (b) Additional filtration by Kodak-Wratten filter No. 12 which transmits less than 1% of light of wavelength less than 500 nm.

topography. Early dust patterns (of which Fig. 9a is an example) revealed not only the visibly darkened patches, but also the well-defined surrounding aureoles. Neither visible examination nor ultra-violet transmission topographs gave any hint of radiation damage outside the small dark patches, but the existence of at least two penumbral zones of low-level radiation damage was confirmed by cathodoluminescence topography. Similar manifestations were observed on all the four large faces: description here will be restricted to one face only. Consider first its cathodoluminescence patterns, illustrated in Fig. 8 with a key shown in Fig. 7. To provide, in monochrome, an indication of spectral distribution in the pattern, the images obtained with a blue-passing filter (Fig. 8a) and with a filter passing wavelengths longer than 500 nm (Fig. 8b) should be compared. The bright network outside the radiation-damaged regions is the blue dislocation luminescence. Most of this comes from the dislocation-rich walls of the mosaic cells (compare with Fig. 11 of [10]), but bright traces of {1 1 1} can also be recognized. Dislocation luminescence is absent from the heavily damaged patches, A_1–A_3 in Fig. 7, much weakened in the inner penumbral zones bounded by B_1, B_2 and B_3, and slightly weakened in the outer penumbra bounded by C. Fig. 8b shows bright coronas of the green-yellow "3H" vibronic emission system [7] surrounding the patches A, and also coming less strongly, but uniformly, from the whole inner penumbra. (This emission has previously been recorded from localized alpha-radiation damaged zones of Type IIb specimens [10].) From the outer penumbra bounded by C another emission mainly associated with radiation damage, the pink "575 nm system", is apparent and, in Fig. 8b, its intensity approximately balances the loss of brightness from the dislocation network.

The powder patterns Fig. 9a and b demonstrate that the three principal levels of radiation damage (in zones A, B and C, respectively) can be differentiated, but no details of the dislocation structure are revealed. The horizontal filamentary streaks in Fig. 9a are artefacts believed to be due to the direction of air current carrying the Pb_3O_4 powder. Some streaks tending from upper right to lower left in Fig. 9b (and also seen in Fig. 10b and 10c) are localized on polishing striae which can be detected microscopically by Nomarski intereference contrast. Rough measurements of the electrical resistivity of the whole specimen block gave the low value 130 ohm m. Clearly the electrical regime in this crystal is very different from that in the specimens previously discussed and the experimental conditions found to be the best for producing contrast reflected this difference. In most cases a current will have been flowing through the specimen during the dusting, and the dust deposition process could appropriately be described as electrophoresis. However, the ratios of relative amount of powder deposited on the several zones varies between techniques. In Fig. 9a there is a simple progression of steps of increasing density in going from A through B and C out to regions not detectably damaged. The technique used in Fig. 9b, on the other hand,

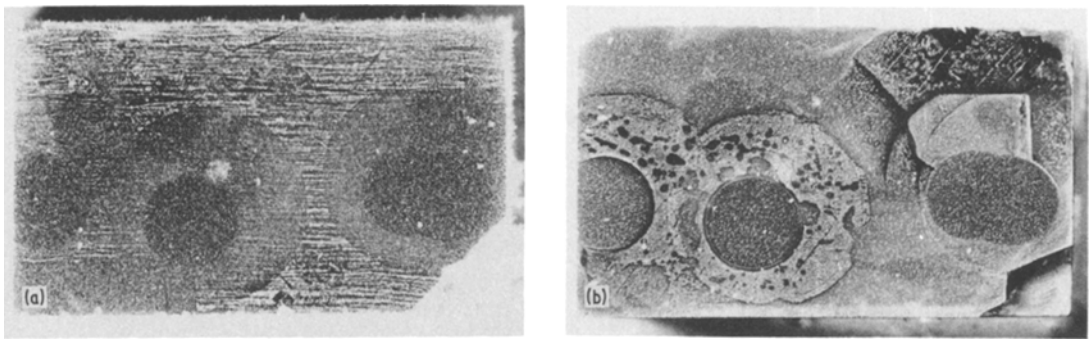

Figure 9 Dust patterns on the surface of the semiconducting diamond shown in Fig. 8. (a) Pb_3O_4 powder, blown from a balloon, with specimen mounted with colloidal graphite on a metal base held at + 5 kV. (b) Magnetic tape developer, specimen mounted in silicone rubber on metal base, corona charging (with some sparking) from a pointed electrode held at − 10 kV.

favoured maximum deposition on the inner penumbra. There is evidence that field gradients at zone boundaries existed which enhanced their visibility, e.g. at the boundary of C in Fig. 9b and of the inner penumbra in Fig. 10a.

The set of patterns Fig. 10a to c, all obtained with MgO smoke, illustrate the variety of patterns obtainable with slighly differing techniques and different weights of powder accumulation. (Heavy deposits become mechanically unstable, and can easily flake off in parts if the specimen is jolted, as occurred in the experiment of Fig. 10c.) Observe that in Fig. 10b and c discrimination between the regions of A_3, depicted as black, and shaded areas in Fig. 7 is effected, and that the outer penumbra is revealed in Fig. 10c but not in the otherwise rather similar pattern Fig. 10b. The sharpness of the boundaries B and C supports their simple geometrical–optical interpretation. (The beam-collimating pinholes were drilled in tantalum sheets 100 μm thick, and three such sheets were spaced out, respectively, at distances roughly 5 cm, 20 cm and 170 cm from the specimen surface [17].) The range of 680 kV protons in diamond is about 3 μm. Absence of detectable colouration in the penumbral zones suggests that the dose there was about two orders of magnitude less than the dose of about 1 μ A h received by the blackened patches. Yet the contrast relative to other regions presented in Fig. 10b and c by the inner penumbral zones

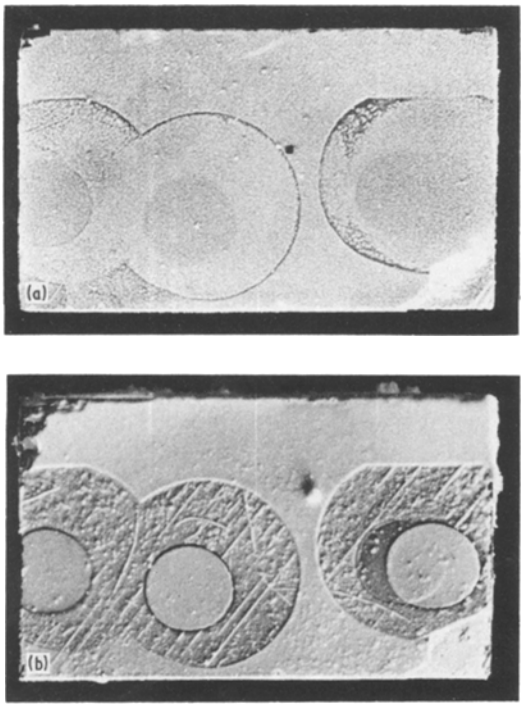

Figure 10 MgO smoke patterns on semiconducting diamond. (a) Specimen mounted with colloidal graphite on a metal base held at + 5 kV. Corona applied from pointed electrode held at − 10 kV. Dust applied 1 sec. after cessation of corona. (b) Procedure as for (a) but with simultaneous application of dust and corona. (c) Specimen mounted using Sellotape on an earthed metal base. Simultaneous application of dust and corona.

(together with the less damaged lune associated with A_3) is noteworthy, and the behaviour in these experiments (in which corona and dust were applied simultaneously) suggests that these penumbral zones were the areas of highest resistivity.

5. Conclusion

The experiments amply demonstrate that dust patterns can be correlated with observations by other crystal characterization techniques such as X-ray topography and cathodoluminescence topography which reveal surface outcrops of internal inhomogeneities. In the present work only well-polished specimen surfaces were used, and it may be doubted whether such good correlation would be obtained in the presence of appreciable surface relief to which electrostatic charging techniques must be especially sensitive. No single "best recipe" for producing dust patterns emerged from this work with regard to the choice of powder; one might perhaps recommend magnetic tape developer for good resolution and MgO smoke for highest contrast.

The results allowing closest approach to simple interpretation were obtained with the Type Ia specimen GH2 which contained Type IIa zones; this specimen represents a common class of inhomogeneity in natural diamonds. On the other hand, observations on the mixed-habit crystal GDO2 add one more puzzle to this complicated crystal-defect phenomenon. Whether the apparently lower resistivity of the {1 1 1} sectors compared with the cuboid sectors arises from excess of platelets and/or "B" nitrogen centres in the former, or from hydrogen in the latter, is a question deserving further study. Explanation is also lacking for the varied phenomena observed, in quite different electrical circumstances, with the semiconductor diamond. But lack of understanding here need not deter exploitation of the technique. Perhaps the results obtained using the semiconductor diamond may spur attempts to apply the method to other semiconducting crystals as a quick, qualitative means for detecting inhomogeneities in resistivity.

References

1. R. C. DeVRIES and R. E. TUFT, *J. Mater. Sci.* **14** (1979) 2650.
2. G. S. WOODS and A. R. LANG, *J. Crystal Growth* **28** (1975) 215.
3. M. SEAL, *Amer. Mineral.* **50** (1965) 105.
4. D. J. CRAIK and R. S. TEBBLE, "Ferromagnetism and Ferromagnetic Domains" (North-Holland, Amsterdam, 1965).
5. G. L. PEARSON and W. L. FELDMAN, *J. Phys. Chem. Sol.* 9 (1959) 28.
6. J. FOUSEK, M. ŠAFRÁNKOVÁ and J. KACZÉR, *Appl. Phys. Lett.* 8 (1966) 192.
7. J. WALKER, *Rep. Prog. Phys.* **42** (1979) 1605.
8. C. D. CLARK, E. W. J. MITCHELL and B. J. PARSONS, in "The Properties of Diamond" edited by J. E. Field (Academic Press, London, New York, 1979) pp. 23–77.
9. M. TAKAGI and A. R. LANG, *Proc. Roy. Soc.* **A281** (1964) 310.
10. P. L. HANLEY, I. KIFLAWI and A. R. LANG, *Phil. Trans. Roy. Soc.* **A284** (1977) 329.
11. E. R. HARRISON and S. TOLANSKY, *Proc. Roy. Soc.* **A279** (1964) 490.
12. F. C. FRANK, in "Science and Technology of Industrial Diamonds" Vol. 1, edited by J. Burls (Industrial Diamond Information Bureau, London, 1967) pp. 119–135.
13. A. R. LANG, *Proc. Roy. Soc.* **A340** (1974) 233.
14. S. SUZUKI and A. R. LANG, in "Diamond Research 1976" (Industrial Diamond Information Bureau, Ascot, 1976) pp. 39–47.
15. *Idem, J. Crystal Growth* **34** (1976) 29.
16. A. R. LANG, *Phil. Mag.* **B41** (1980) 689.
17. COLLINS, private communication (1980).

Received 13 August and accepted 15 September 1980.